Int. J. Heat Mass Transfer. Vol. 36, No. 5, pp. 1231–1240, 1993
Printed in Great Britain

0017–9310/93 $6.00 + 0.00

Impeded natural convection in a rotating, radial tube

G. S. H. LOCK and LITONG ZHAO
Department of Mechanical Engineering, University of Alberta, Edmonton, Alberta, Canada T6G 2G8

(*Received* 13 *January* 1992 *and in final form* 29 *May* 1992)

Abstract—This paper is concerned with single-phase natural convection in a short, square-section, radial tube rotating under steady, laminar conditions. The differential equations governing continuity, momentum and energy in a rectangular cavity rotating about a vertical axis at various speeds are solved numerically using a finite-difference algorithm. Results have been obtained for impeded flow with representative values of the principal nondimensional groups: Rayleigh number, acceleration ratio, Ekman number, Prandtl number (100), eccentricity ratio (100) and aspect ratio (5:1). The data obtained revealed the complex effect of the Coriolis acceleration on flow and heat transfer when the tube wall temperature increased linearly with radius.

1. INTRODUCTION

ONE OF THE earliest practical applications of natural convection in the removal of heat from rotating machinery is provided by the thermosyphon cooling system proposed by Schmidt [1]. This was designed to permit higher working temperatures in gas turbines by using hollow blades sealed at the tip but opening at the root into a drum containing a liquid coolant. Under high centrifugal accelerations, typically of the order of $10^4 g$, the liquid coolant not only fills the blade cavities but circulates under the influence of thermally induced buoyancy forces created by the internal temperature field. It is thus possible to produce very high convective fluxes inside the blade and thereby keep its exterior relatively cool, at least in principle.

Various practical difficulties with this ingenious scheme [2] led to it being succeeded by another in which the basic idea was retained but the details changed. Specifically, the open mouth was abandoned and replaced by a tubular extension of the blade cavity which was then completely sealed after first being charged with a suitable coolant. The heat transferred from the hot gases surrounding the blade continues to be removed by a convective flux, but this now penetrates into the tubular extension, the principal design difference being the subsequent removal of this heat by external cooling provided within the drum.

Given this application of the radial thermosyphon to high speed gas turbines, it is perhaps not surprising that attention was focused initially on behaviour near the fluid critical pressure [3]. Above this pressure, the internal circulation is driven by thermal buoyancy, while below it the circulation is driven by Archimedean buoyancy in the presence of a phase change. Generally speaking, the latter is much greater than the former except near the critical pressure when the coefficient of thermal expansion $\beta \to \infty$.

The static simulation of two-phase behaviour in rotating thermosyphons has been inconclusive [4], and indeed fundamental characteristics continue to unfold [5, 6]. There appear to be no comparisons of tilted and radial evaporative thermosyphons which test the conventional wisdom that a lateral body force component (from gravity) acts in a similar way to the Coriolis acceleration, despite the fact that the former is uniformly pervasive while the latter depends directly on the fluid velocity, i.e. independently of buoyancy [7].

Under single-phase conditions, the situation is less complex because the influence of the Coriolis acceleration is no longer felt at a liquid–vapour interface where it is capable of altering both the shape and the stability characteristics; nor is the influence felt in the processes accompanying boiling [8]. The non-evaporative, radial thermosyphon separates these effects from the more general effects incorporated in the equation of motion. Understanding of the simpler system thus leads to an understanding of the more complex system. Equally important is the single-phase system in its own right. By their nature, tubular thermosyphons transmit longitudinal convective fluxes which are much larger than the equivalent conductive flux under the same thermal conditions, and this is true even for single-phase natural convection. Single-phase thermosyphons are useful whenever the thermal resistance they establish is small in relation to the flanking resistances with which they are in series. Single-phase, radial thermosyphons therefore have a potential role to play, on Earth or in space, whenever their conductances are high enough for the designer to benefit from their comparative simplicity.

In this paper, a radial thermosyphon in the shape of a rectangular cavity will be studied in its simplest and most conservative form; namely, single-phase natural convection under steady laminar conditions. The purpose is to use a numerical analysis to reveal

NOMENCLATURE

A	area
D	width
Ek	Ekman number
g	gravitational acceleration
k	thermal conductivity
L	length
Nu	Nusselt number
P, p	absolute (nondimensional) pressure
Pr	Prandtl number
Q	heat
R	radius
$\mathscr{R}$	root radius
T	absolute temperature
U, u	axial (nondimensional) velocity
V, v	radial (nondimensional) velocity
W, w	tangential (nondimensional) velocity
X, x	axial (nondimensional) displacement
Y, y	radial (nondimensional) displacement
Z, z	tangential (nondimensional) displacement.

Greek symbols

β	thermal expansion coefficient
η	acceleration ratio
θ	temperature difference
κ	thermal diffusivity
ν	momentum diffusivity
ρ	density
ϕ	nondimensional temperature
Φ	azimuthal displacement
Ω	rotational speed.

Subscripts

C	cooled
H	heated
m	mid length
o	reference
X, etc.	differentiation with respect to X, etc.

Superscript

$\cdot$	per unit time.

the circulation set up in a viscous liquid under the influence of a tube wall temperature increasing linearly with radius. In particular, the results will be used to describe both the primary and the secondary flow and their influence on heat transfer. This permits comparisons with the tilted gravitational system. It also elucidates the role of the Coriolis acceleration and thereby tests the conventional wisdom.

2. PHYSICO-MATHEMATICAL DESCRIPTION

The most natural way to describe incompressible fluid motion in a rotating system is to use a system of coordinates which rotates synchronously with the system itself. For a radial thermosyphon rotating steadily at a speed Ω about a vertical axis, the governing equations then take the following form [9].

Continuity

$$\nabla \cdot \mathbf{V} = 0.$$

Motion

$$\rho(\mathbf{V}\cdot\nabla)\mathbf{V} + 2\rho\boldsymbol{\Omega}\times\mathbf{V} = -\nabla P - \rho\beta\theta[\mathbf{g} - \boldsymbol{\Omega}\times(\boldsymbol{\Omega}\times\mathbf{R})] + \mu\nabla^2\mathbf{V}$$

in which the Boussinesq approximation has been invoked, and $\theta = T - T_0$, where T_0 is a reference temperature at which the fluid is isothermally at rest.

Energy

$$\rho c_p(\mathbf{V}\cdot\nabla)\theta = k\nabla^2\theta$$

in which compression work and energy dissipation are ignored.

These equations apply to the short, rectangular cavity depicted in Fig. 1. The vertical coordinate X is measured upwards while the tangential coordinate Z is measured clockwise from beneath, increasing from the trailing to the leading face. The length of the cavity L is taken to be much greater than its width D; the ratio is here fixed at 5 : 1. The governing equations may thus be written in a rotating, rectangular Cartesian system of coordinates as follows:

Continuity

$$U_X + V_Y + W_Z = 0. \tag{1}$$

Axial momentum

$$UU_X + VU_Y + WU_Z = -\frac{1}{\rho}P_X + \beta\theta g + \nu(U_{XX} + U_{YY} + U_{ZZ}). \tag{2}$$

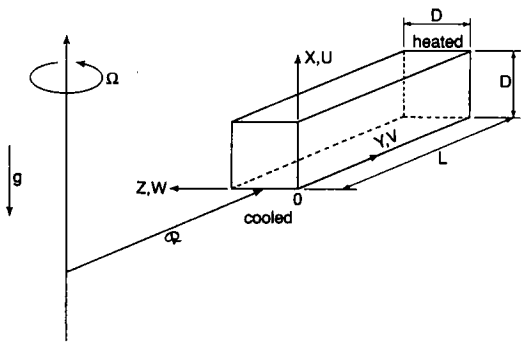

FIG. 1. Coordinate system for rotating tube.

Radial momentum

$$UV_X+VV_Y+WV_Z-2\Omega W=-\frac{1}{\rho}P_Y-\beta\theta\Omega^2(\mathscr{R}+Y)+\nu(V_{XX}+V_{YY}+V_{ZZ}). \quad (3)$$

Tangential momentum

$$UW_X+VW_Y+WW_Z+2\Omega V=-\frac{1}{\rho}P_Z-\beta\theta\Omega^2\left(Z-\frac{D}{2}\right)+\nu(W_{XX}+W_{YY}+W_{ZZ}). \quad (4)$$

Energy

$$U\theta_X+V\theta_Y+W\theta_Z=\kappa(\theta_{XX}+\theta_{YY}+\theta_{ZZ}). \quad (5)$$

The boundary conditions to be satisfied are: $U=V=W=0$ on all enclosing planes and $\theta=T-T_m=\theta^c(2Y/L-1)/2$ on the side planes, where $\theta^c=T_H-T_C$ is the overall temperature difference between the ends and $T_m=(T_H+T_C)/2$ is the average (mid-length) wall temperature. The thermal boundary condition represents perfectly conducting cavity walls and is most appropriate to a thermosyphon for which the heated and cooled sections are not separated by thermal insulation.

3. NUMERICAL FORMULATION

Prior to attempting a solution of equations (1)–(5), each of the primitive variables contained therein was re-cast in non-dimensional form through the use of the following definitions

$$x=\frac{X}{D},\quad y=\frac{Y}{L},\quad z=\frac{Z}{D}$$

$$u=\frac{UL}{D\sqrt{F}},\quad v=\frac{V}{\sqrt{F}},\quad w=\frac{WL}{D\sqrt{F}}$$

$$p=\frac{P}{\rho F}\quad\text{and}\quad\phi=\frac{2(T-T_m)}{T_H-T_C}$$

where

$$F=\beta\Omega^2(\mathscr{R}+L)(T_H-T_C)\frac{L}{2}$$

measures the thermal buoyancy, the driving force. With the exception of coordinates and the temperature, the above variables are not, in general, normalized; the range of conditions covered below is too great to expect uniform normalization from a single choice of scales. However, the selection of appropriate scales for particular conditions will be used later to discuss the particulars of system behaviour. Substitution into the governing equation thus reveals six controlling parameters: Prandtl number Pr, here fixed at 100 to represent a viscous liquid; aspect ratio L/D, fixed at 5:1; eccentricity ratio $\mathscr{R}/L$; acceleration ratio $\Omega^2(\mathscr{R}+L)/g$; Ekman number $Ek=\nu/\Omega D^2$ and Rayleigh number $Ra=\beta\Omega^2(\mathscr{R}+L)(T_H-T_C)D^3/\nu\kappa$. More will be said about these parameters in the next section. At this point it is sufficient to note the great variability, even within the limited problem posed.

The resulting nondimensional equations were solved using the SIMPLE-C finite-difference algorithm [10, 11], treating buoyancy as a source term. The solutions were deemed to have converged when two successive iterations produced agreement within 0.5% in the dependent variables. Following previous experience [12, 13] a $15\times51\times15$ non-uniform network was used to generate field data from which the Nusselt number was calculated according to the definition

$$Nu=\frac{\dot{Q}L}{Ak(T_H-T_C)} \quad (6)$$

where $\dot{Q}$ is the total heat flux into, through and out of the cavity, and A is half the total surface area, i.e. $A=D^2+2LD$. Typically, 2 h CPU time on a FPS 164 computer were required for each converged data point.

Essentially the same programme has been used successfully in similar work [13, 14] prior to which it was validated both qualitatively and quantitatively. The flow details presented below are therefore considered to be correct. The accuracy of the Nusselt number has been estimated at about 5%, the maximum difference between the calculated heat input and output. No check of mesh independence was made for these non-uniform mesh data, but a comparable test for an eccentric thermosyphon with a uniform grid confirms the accuracy estimate.

4. DISCUSSION AND RESULTS

Since seven parameters have been identified it is clear that a systematic survey of each is beyond a single study. The discussion below is therefore restricted to a survey of regime behaviour so as to provide a rational basis for future work. The geometry is defined by the square-section and a length–width ratio of 5:1. The fluid is taken to have constant properties with a Prandtl number of 100, characteristic of viscous liquids, and the eccentricity ratio $\mathscr{R}/L$ is fixed at 100:1 with the axis of rotation being vertical. Only brief consideration will be given to the effects of Pr and $\mathscr{R}/L$. This essentially limits discussion to the effects of three parameters on heat transfer rate: the Rayleigh number in the laminar range $10^3<Ra<10^7$; the Ekman number in the lower speed range $10^{-4}<Ek<10^{-1}$; and the acceleration ratio in the practical range $1<\eta<100$.

4.1. *The effect of Rayleigh number*

The effect of Rayleigh number on heat transfer is shown in Fig. 2 with $Ek=5\times10^{-3}$ and $\eta=100:1$. Also shown (circles) is the numerical data of Lock and Zhao [15] for the same cavity standing vertically at rest (with $\Omega^2(\mathscr{R}+L)$ replaced by g in the Rayleigh number). Since the vertical cavity experiences neither

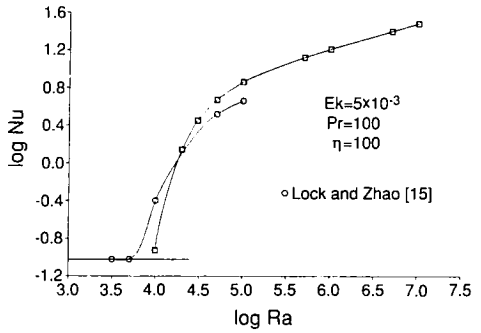

FIG. 2. Effect of Rayleigh number on heat transfer.

a lateral gravitational component nor the effect of Coriolis forces, the comparison provides a measure of the latter in the rotating cavity. In the vicinity of $Ra = 10^5$, the Coriolis forces evidently improve the heat transfer rate slightly. This is probably caused by the accompanying secondary flow but the performance reversal at $Ra = 10^4$, for example, suggests that a simple explanation may not exist.

In general terms, the data of Fig. 2 reveal three different regimes. For low Rayleigh numbers, e.g. $Ra < 10^4$, the Nusselt number is at, or very close to, the conduction limit $Nu = 1/11$, according to the definition given earlier. Under these conditions, the velocity field has little influence on the conductive temperature field. Near the upper reaches of the regime, however, the temperature field does influence the velocity field. In particular, it influences the stability and evolution of the mid-length thermal exchange mechanism as it changes from pure conduction to pure convection [5, 16, 17]. The lowest data for the rotating cavity, although shown as part of a continuous curve, were not the only converged results obtained in the region. A few other points (not shown) representing alternative stable, though perhaps not unique, solutions suggested that the thermal exchange mechanism may be especially susceptible to slight shifts in the presence of Coriolis forces; in particular, the organization of convective filaments carrying hot and cold streams may be influenced by the Coriolis effect. Only a fully transient solution could provide a complete description of these bifurcations which, being sensitive to initial conditions, stand in sharp contrast to all the other data of this paper.

For much higher Rayleigh numbers, e.g. $Ra > 10^6$, the rotating cavity data are reminiscent of a laminar boundary layer regime. In its upper reaches, the curve shown appears to be asymptotic to a line of slope 0.25, but some difficulties with convergence again sound a note of caution. Under these conditions, the convective exchange mechanism in the mid-length region is well established in a bifilamental form, as demonstrated below. However, the role of the Coriolis forces may be expected to increase within the boundary layer as it becomes thinner and moves faster. This is particularly true over the upper and lower surfaces where the Ekman layers operate. Such a development at very high Rayleigh numbers may thus preclude the existence of the classical boundary layer regime observed in stationary thermosyphons [18].

Between the upper limit of the conduction regime at $Ra \simeq 10^4$ and the lower limit of the boundary layer regime at $Ra \simeq 10^5$ is an intermediate regime. In gravitational thermosyphons, corresponding limits have been used to define the *impeded* regime [13, 18]. This is the principal regime of interest in this paper. For stationary cavities, the slope of the $Nu \simeq Ra$ curve is equal to, or slightly less than, 1.0 under laminar impeded conditions. Figure 2 reveals that this is not true for the rotating cavity considered here. It appears that as the Rayleigh number is lowered beneath 10^5, the effect of the Coriolis forces is to accelerate entry into the conduction regime, thus steepening the slope. All of the corresponding data on the curve shown in Fig. 2 represent stable solutions. One point in the middle of these impeded data, specifically at $Ra = 5 \times 10^4$, will be used as a reference when investigating the effects of other parameters below.

Under these particular conditions, Fig. 3 displays the velocity field in a longitudinal, horizontal plane lying in the mid-X plane of rotation. By analogy with a vertical thermosyphon, this reveals that the deep flow, i.e. near the closed ends, has an annular refluent form; that is, fluid near the side walls flows towards the mid-length position while central cores flow away from it. Away from the ends, however, the flow is evidently bifilamental with hot fluid moving radially inward over the leading face to supply the core in the cooled section while cold fluid moves radially outward over the trailing face to supply the heated section core.

The extent of the bifilamental region is greater than might be expected in a vertical thermosyphon, but is reminiscent of that found in the tilted thermosyphon [13] where the lateral component of the gravitational field creates a secondary flow. Here, it is the Coriolis acceleration which plays a similar role; for example, by causing the radially inward moving annulus of fluid in the heated section to collect along the leading face. This behaviour supports the conventional wisdom on the effect of Coriolis forces, at least in a qualitative sense, but a more thorough appraisal will be given later.

Figure 4 shows the relative contributions to the overall heat transfer rate attributable to each of the individual surfaces of the cavity. In the boundary layer regime, all the surfaces evidently make very similar contributions. In the conduction regime, the end surface eventually dominates, although this is not clear from the figure, given the Nusselt number scale chosen. In the impeded regime, it is the trailing face which makes the greatest contribution, matched only by the combined effect of the upper and lower faces where the Ekman layers are located. At first thought, this is a surprising result, given the anticipated role of the Coriolis acceleration in the Ekman layers. To

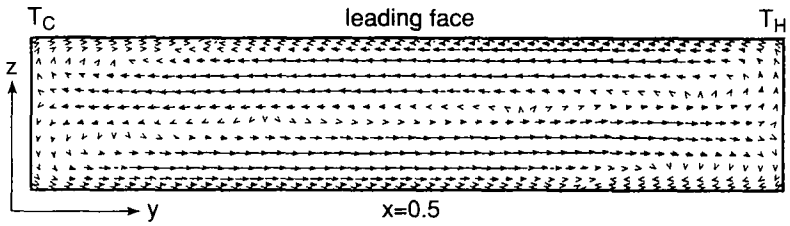

FIG. 3. Longitudinal velocity field in mid-plane of rotation.

understand the reason behind this finding it is necessary to consider the role of the Ekman number.

4.2. *The effect of Ekman number*

As the Ekman number increases, the effect of the Coriolis acceleration decreases; for a sufficiently large Ekman number the Coriolis effect may be ignored. Consider the consequence of decreasing the Ekman number when the Coriolis effect is weak. It is to be expected that the Ekman layers would then begin to play an increasing part in the secondary flow, thus increasing the heat transfer rate; that is, the Coriolis effect would be analogous to tilting a vertical cavity. Under these conditions, the contributions of the Ekman layers to the heat transfer rate may be estimated from a scaling analysis of equations (1)–(5).

A balance between the thermal buoyancy and the largest viscous term in the radial equation of motion implies that

$$\frac{\nu V^c}{(X^c)^2} = 0(\beta\theta^c\Omega^2\mathscr{R}) \tag{7}$$

where the superscript c indicates the scale of the variable. Likewise, a balance between the Coriolis acceleration and the largest viscous term in the Ekman layer implies that

$$\frac{\nu W^c}{(X_E^c)^2} = 0(2\Omega V^c) \tag{8}$$

where X_E^c is the thickness scale of the Ekman layer. In general, $X_E^c \leqslant X^c$, the thickness of the primary flow layer on which the Ekman layer depends. Consider the consequence of $X_E^c = X^c$ when a thermal balance completes the essential description. Equating the heat supplied conductively to each Ekman layer to that removed convectively

$$\frac{\kappa}{(X^c)^2} = 0\left(\frac{W^c}{Z^c}\right) \tag{9}$$

where $Z^c = 0(D)$, the cavity width.

Equations (7)–(9) yield the following scales

$$X_E^c = D\left(\frac{Ek}{2Ra}\right)^{1/6} \tag{10}$$

$$V^c = \frac{k}{D}\left(\frac{Ra^2\,Ek}{2}\right)^{1/3} \tag{11}$$

$$W^c = \frac{k}{D}\left(\frac{2Ra}{Ek}\right)^{1/3} \tag{12}$$

from which the heat transfer through the Ekman layers may be determined. Thus

$$Nu = C_1\left(\frac{Ra}{Ek}\right)^{1/6} \tag{13}$$

where C_1 is an empirical coefficient.

This result suggests that the Ekman layers reflect the augmentation of heat transfer in the presence of a weak Coriolis effect, when the heat transfer will increase as the Ekman number decreases. Such a Coriolis-enhanced regime is evident in Fig. 5 which

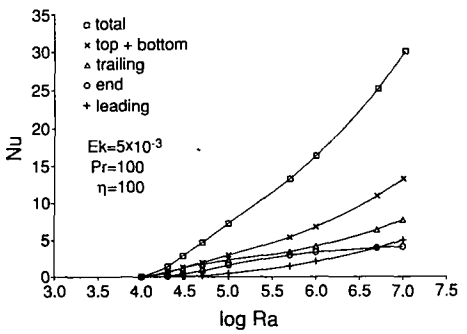

FIG. 4. Components of the overall heat transfer rate.

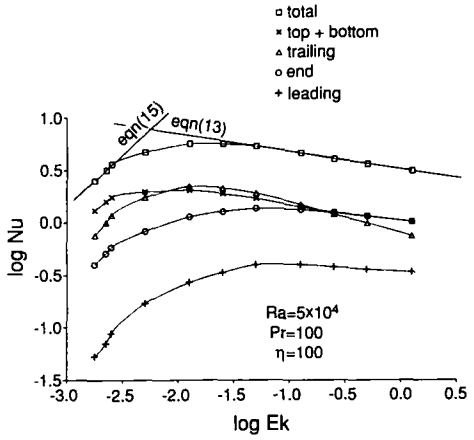

FIG. 5. Effect of Ekman number on heat transfer.

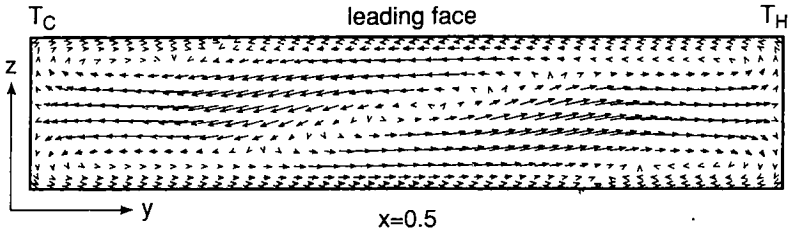

FIG. 6. Longitudinal velocity field in mid-plane of rotation.

shows numerical data covering the range $2 \times 10^{-3} < Ek < 1.0$; an asymptote based on equation (13) is shown against the high Ek data. Figures 6 and 7 show the primary flow under these conditions. Both figures reveal that the flow deep within the cavity, i.e. near the closed ends, has an annular form reminiscent of a vertical cavity. The Coriolis effect induces fluid leaving the cold end to collect along the trailing face while warmer fluid coming from the hot end collects along the leading face. This tendency converts the deep annular pattern into the mid-length bifilamental pattern shown.

Figure 5 reveals that the enhancing effect of the Ekman layers does not continue indefinitely. As the Ekman number decreases, this regime is succeeded by another with the opposite effect, and more appropriately described as a Coriolis-impeded regime. The role of the Ekman layers in this lower regime continues to be strong, as evidenced by the form of equation (10) and the contribution of the top and bottom surfaces seen in Fig. 5. However, it is the trailing face which then provides the best measure of the effect of Ekman number in conditions where the Coriolis acceleration, acting tangentially, creates a substantial alteration in the pressure field. While this effect is roughly analogous to that found in highly tilted (near horizontal) gravitational systems, it acts to oppose the main flow and thus denies the conventional wisdom based on the analogy.

In a geophysical context, this situation corresponds to a geostrophic flow in which the effect of the pressure gradient is balanced by the Coriolis effect. A scaling analysis of equations (1)–(5) again provides some insight.

Elimination of the pressure from the radial and tangential equations of motion yields a balance between the three principal terms; thus

$$\beta\Omega^2\mathscr{R}\theta_Z - \nu V_{ZZZ} = 0(2\Omega V_Y)$$

from which the corresponding velocity and thickness scales are found to be

$$V^c = \frac{\kappa}{D} Ra \left(\frac{L\,Ek}{2D}\right)^{2/3}$$

and

$$Z^c = D\left(\frac{L\,Ek}{2D}\right)^{1/3}. \tag{14}$$

These correspond to a two-dimensional primary flow field independent of axial location X, and for which the heat transfer rate through the trailing face is given by

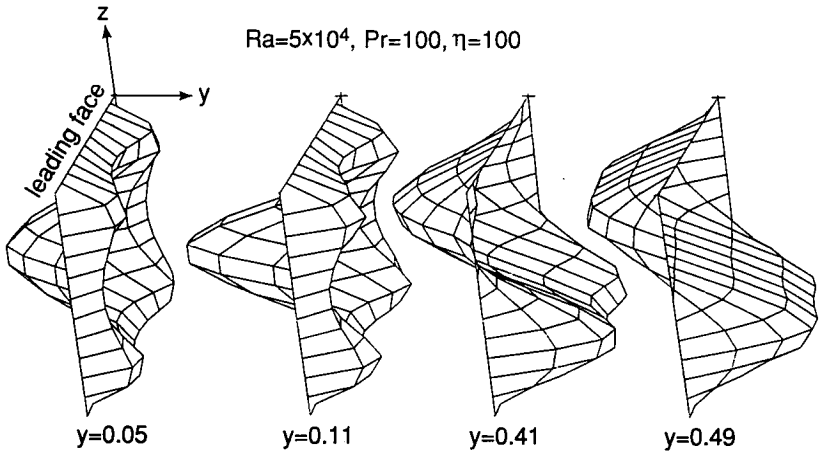

FIG. 7. Development of velocity profile: $Ek = 2.5 \times 10^{-2}$.

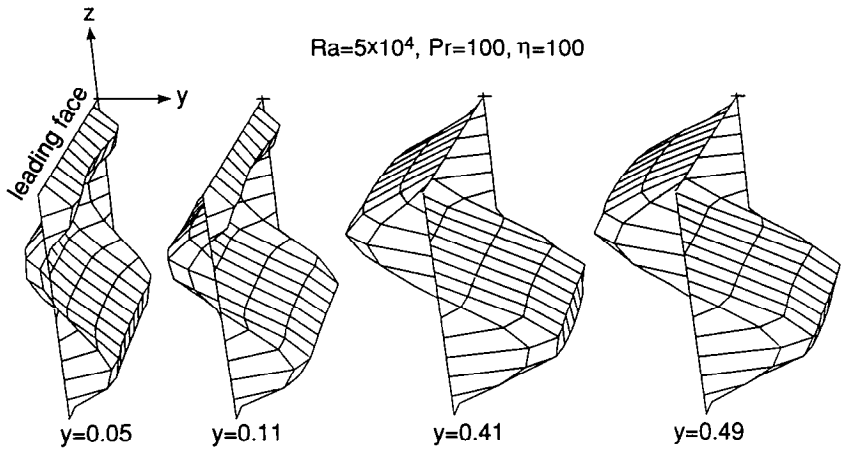

FIG. 8. Development of velocity profile: $Ek = 5 \times 10^{-3}$.

$$Nu = C_2 \, Ra \, Ek \tag{15}$$

where C_2 is an empirical coefficient. This result contrasts strongly with that given by equation (13), and illustrates the result of Coriolis forces large enough to control the tangential pressure gradient. An asymptote based on equation (15) is shown in Fig. 5.

Figures 8 and 9, together with Fig. 3, describe the velocity field in this impeded regime. From Fig. 8, it is evident that the primary flow is almost two-

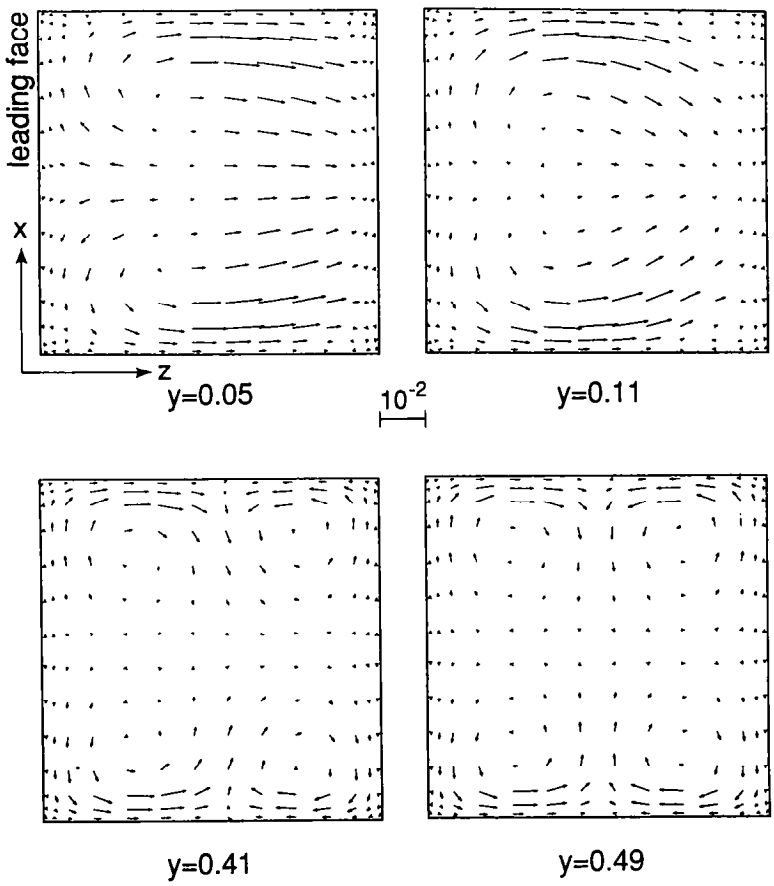

FIG. 9. Development of transverse velocity field: $\eta = 100$.

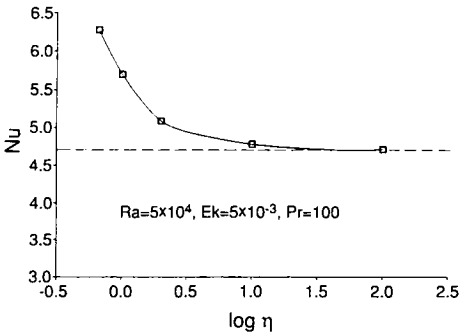

FIG. 10. Effect of acceleration ratio on heat transfer.

dimensional, as anticipated. However, it is clear from Fig. 9 that a secondary flow continues to exist. The deep flow again reveals a stagnation point from which fluid no longer radiates axisymmetrically. Instead, it flows more or less in the planes of rotation under the influence of strong Coriolis forces. Vortices appearing at the corners flanking the leading face grow with distance from the closed end until, at the mid-length plane, they form one of two symmetric pairs. The Ekman layers are thus preserved.

4.3. *The effect of acceleration ratio*

The above results were obtained with an acceleration ratio $\eta = \Omega^2(\mathscr{R}+L)/g \gg 1$. The effect of reducing this ratio while maintaining $\mathscr{R} \gg L$, is shown in Fig. 10 which reveals that the Nusselt number asymptote is almost reached when $\eta \leqslant 10$; the previous neglect of gravity is thus justified *a posteriori*. When $\eta \ll 10$, gravity exerts an influence in two ways: on the secondary flow through direct thermal buoyancy; and on the primary flow through indirect thermal buoyancy. In the limit as $\eta \to 0$, system behaviour reverts to that of a stationary horizontal cavity, but this cannot be shown on Fig. 10 which is constructed with fixed values of Ra and Ek. For a fixed geometry, decreases in η are attributable only to decreases in speed Ω, at least on this planet. The increase in Nusselt number found as η decreases evidently has two main causes: an increase in $D^3(T_H - T_C)/\nu\kappa$, from the Rayleigh number restriction, and a decrease in ν/D^2, from the Ekman number restriction.

Figures 11 and 12 show the flow field for $\eta = 1$ with $Ra = 5 \times 10^4$, $Ek = 5 \times 10^{-3}$ and $\mathscr{R}/L = 100$. In both of these, the twisting effect of gravity is revealed. This stems from the superposition of two lateral force fields which are mutually perpendicular: Coriolis forces act tangentially in planes of rotation, while direct thermal buoyancy acts vertically. Their combined effect obviously varies with η, the resulting lateral field gradually rotating through 90° as η decreases from very large to very small values, or vice versa.

By comparison with Fig. 8, the primary flow field shown in Fig. 11 is no longer quasi-two-dimensional, the change being greatest nearer the closed ends. Likewise, by comparison with Fig. 9, the secondary flow field shown in Fig. 12 is no longer symmetric about the mid-X plane of rotation. The augmentation of the downward flow of cooled fluid near the leading edge is clearly evident deep within the cavity. At the mid-length plane, direct thermal buoyancy now creates an anti-symmetry not unlike that observed in a square-section cavity with its sides inclined [19].

5. CONCLUSIONS

This paper provides a numerical analysis of a square-section, radial cavity rotating about a vertical axis. The governing differential equations for continuity, momentum and energy have been solved using a finite-difference algorithm in a set of coordinates rotating synchronously. The equations were given a rectangular formulation appropriate to steady, laminar flow subject to the Boussinesq approximation. Solutions were then obtained iteratively for a $15 \times 51 \times 15$ network. Convergence required successive agreement of better than 0.5% in the dependent variables.

Nondimensionalization of the governing equations revealed that the heat transfer rate could be expressed in a fairly general relation of the form

$$Nu = f\left(Ra, Ek, \eta, Pr, \frac{\mathscr{R}}{L}, \frac{L}{D}\right).$$

By choosing $Pr = 100$ and fixing the geometry and orientation of the cavity, it was possible to study the behaviour of viscous liquids under representative conditions. In particular, the role of the Coriolis effect has been explored under low speed conditions.

The effect of Rayleigh number on heat transfer revealed three well-established regimes: a conduction regime and a boundary layer regime separated by an impeded regime, the latter being the focus of this paper. The effect of the Ekman number was to complicate this classical description of regimes. Even within the restriction of impeded flow, it was found that the Ekman number introduced at least two further regimes. At higher values of Ek (lower speeds), the Ekman layers improved heat transfer rates in what has been called the Coriolis-enhanced regime. At lower values of Ek (higher speeds), the Ekman layers were unable to prevent a general deterioration in performance in a Coriolis-impeded regime.

The Coriolis-enhanced regime is not unlike that found in cavities tilted slightly from the vertical. This behaviour is in keeping with the conventional wisdom which presumes an analogue, even though Coriolis forces (in the rotating system) are not directly dependent on the temperature field while lateral buoyancy forces (in the stationary system) are. To extend this 'analogy' to higher speeds or greater tilts appears to be a gross error. While both show a performance deterioration attributable to a modified longitudinal pressure gradient, the rotating system tends to produce a flattened velocity field which decays, theoretically, to zero as $Ek \to 0$.

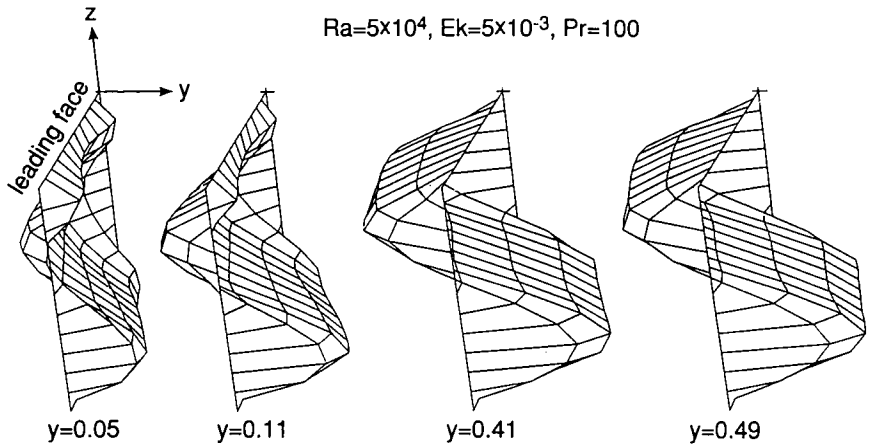

FIG. 11. Development of velocity profile: $\eta = 1$.

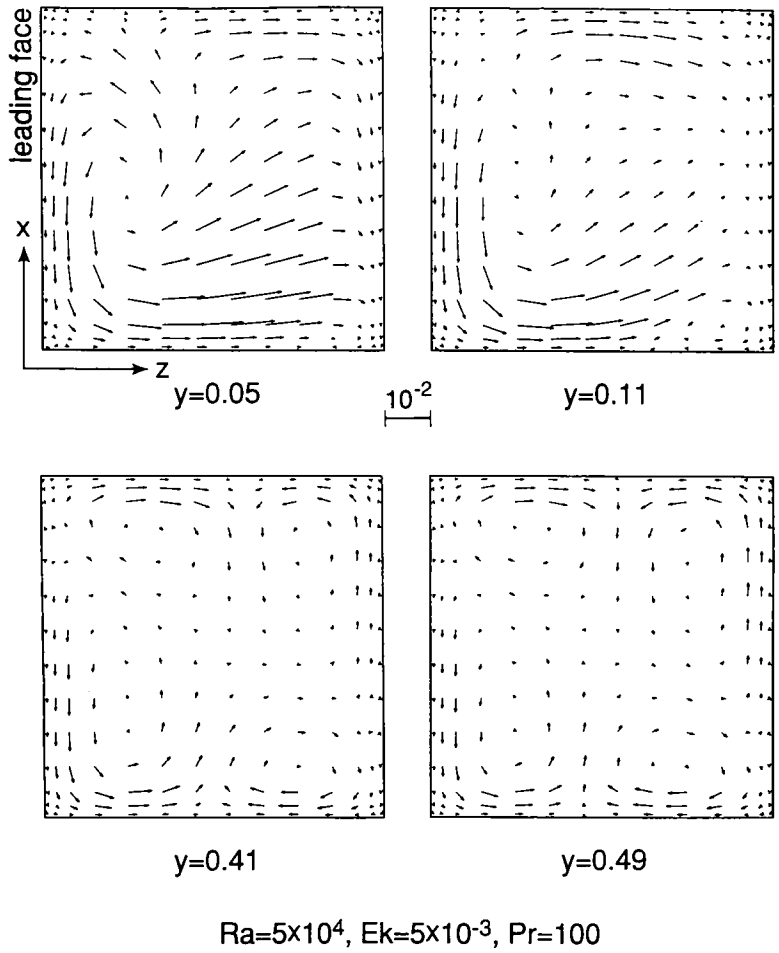

FIG. 12. Development of the transverse velocity field: $\eta = 1$.

The effect of reducing the acceleration ratio was also found to be complex. With $\eta = 1$, it was found that the vertical gravitational acceleration combined with the tangential (horizontal) Coriolis acceleration twisted the flow field. This alteration in the secondary flow field increased the heat transfer rate, signalling the benefits of low speed rotation.

Acknowledgement—This work was performed under the auspices of the Natural Sciences and Engineering Research Council of Canada to whom we are indebted.

REFERENCES

1. E. Schmidt, Heat transmission by natural convection at high centrifugal acceleration in water-cooled gas turbine blades, *General Discussion on Heat Transfer, Proc. I. Mech. E.*, London, Vol. IV, pp. 361–363 (1951).
2. H. Cohen and F. J. Bayley, Heat transfer problems of liquid-cooled gas turbine blades, *Proc. I. Mech. E.*, London, Vol. 169(20), pp. 1063–1080 (1955).
3. E. Schmidt, Wärmetransport Durch Natürliche Konvektion in Stoffen Bei Kritischem Zustand, *Int. J. Heat Mass Transfer* **1**, 92–101 (1960).
4. P. Palanikumar, The effect of tube inclination on heat transfer in the closed, evaporative thermosyphon, M.Sc. Thesis, University of Durham, England (1960).
5. D. Japikse, Advances in thermosyphon technology. In *Advances in Heat Transfer*, Vol. 9, pp. 1–111. Academic Press, New York (1973).
6. K. Negishi and T. Sawada, Heat transfer performance of an inclined, two-phase closed thermosyphon, *Int. J. Heat Mass Transfer* **26**(8), 1207–1213 (1983).
7. G. S. H. Lock, *The Tubular Thermosyphon*. Oxford University Press, Oxford (1992).
8. I. A. Mudawwar and M. A. El-Masri, Boiling incipience in plane rotating water films, *J. Heat Transfer* **110**, 532–535 (1988).
9. H. P. Greenspan, *The Theory of Rotating Fluids*. Cambridge University Press, Cambridge (1969).
10. S. V. Patankar, A circulation procedure for two-dimensional elliptic equations, *Numer. Heat Transfer* **4**, 409–425 (1981).
11. J. P. van Doormaal and G. D. Raithby, Enhancements of the SIMPLE method for predicting incompressible fluid flows, *Numer. Heat Transfer* **7**, 147–163 (1984).
12. P. Bontoux, B. Roux, G. H. Shiroky, B. L. Markham and F. Rosenberger, Convection in the vertical midplane of a horizontal cylinder. Comparison of two-dimensional approximations with three-dimensional results, *Int. J. Heat Mass Transfer* **29**, 227–239 (1986).
13. G. S. H. Lock and J.-C. Han, Buoyant laminar flow of air in a long, square-section cavity aligned with the ambient temperature gradient, *J. Fluid Mech.* **207**, 489–504 (1989).
14. G. S. H. Lock and J.-C. Han, The effects of tilt, skew and roll on natural convection in a slender, laterally-heated cavity, *Math. Comput. Modelling* **13**(2), 23–32 (1990).
15. G. S. H. Lock and Litong Zhao, The laminar flow field in a near-vertical, closed tube thermosyphon, *Proc. 7th Int. Conf. on Math. and Comput. Model.*, Chicago, Vol. 14, pp. 822–825 (1990).
16. F. J. Bayley and G. S. H. Lock, Heat transfer characteristics of the closed thermosyphon, *J. Heat Transfer* **87**, 30–40 (1965).
17. G. D. Mallinson, A. D. Graham and G. de Vahl Davis, Three-dimensional flow in a closed thermosyphon, *J. Fluid Mech.* **109**, 259–275 (1981).
18. M. J. Lighthill, Theoretical considerations on free convection in tubes, *Q. J. Mech. Appl. Math.* **VI**(4), 398–439 (1953).
19. G. S. H. Lock and Litong Zhao, Natural convection in honeycomb wall spaces, *Int. J. Heat Mass Transfer* **35**, 155–164 (1992).